



2011-01

Vision-Based Tracking and Motion Estimation for Moving Targets Using Small UAVs

Dobrokhodov, Vladimir N.



Calhoun is a project of the Dudley Knox Library at NPS, furthering the precepts and goals of open government and government transparency. All information contained herein has been approved for release by the NPS Public Affairs Officer.

**Dudley Knox Library / Naval Postgraduate School
411 Dyer Road / 1 University Circle
Monterey, California USA 93943**

Vision-Based Tracking and Motion Estimation for Moving Targets Using Small UAVs

Vladimir N.Dobrokhodov^{*}, Isaac I.Kaminer[†] and Kevin D.Jones[‡]
Naval Postgraduate School, Monterey, CA 93943

Reza Ghabcheloo[§]
Instituto Superior Tecnico (IST), Lisbon, Portugal

This paper addresses the development of a vision-based target tracking system for a small unmanned air vehicle. The algorithm performs autonomous tracking of a moving target, while simultaneously estimating GPS coordinates, speed and heading of the target. Tight real-time integration of UAV's video and telemetry data-streams with geo-referenced database allows for reliable target identification, increased precision and shortened time of target motion estimation. A low cost off the shelf system is utilized, with a modified radio controlled aircraft airframe, gas engine and servos. Tracking is enabled using a low-cost, miniature pan-tilt gimbal. The control algorithm provides rapid target acquisition and tracking capability. A target motion estimator was designed and shown in multiple flight tests to provide reasonable targeting accuracy. The impact of tracking loss events on the control and estimation algorithms is analyzed in detail.

Nomenclature

H	=	Jacobian of nonlinear transformation
${}^I R_C, {}^I R_B, {}^B R_C$	=	coordinate transformation matrixes
$\{I\}, \{B\}, \{C\}$	=	inertial, body and camera coordinate frames
\vec{V}, V, \mathbf{V}	=	the airplane velocity vector and its magnitude
\vec{V}_g, V_g	=	the airplane ground velocity speed vector and its magnitude
\vec{V}_p	=	velocity vector tangent to the line of sight (LOS)
$\vec{V}_t, V_t, \hat{\mathbf{V}}_t$	=	target velocity vector, its magnitude an estimate
c_ρ	=	parameter characterizing region of attraction
e_1, e_2	=	stability margins
f	=	focal length of the camera
$g_{\varphi\theta}$	=	nonlinear transformation
k_1, k_2	=	feedback control law coefficients
K_1, K_2	=	nonlinear estimator coefficients
$\mathbf{p}, \hat{\mathbf{p}}$	=	vector, position of target w/r to UAV and its estimate
\mathbf{p}_b	=	vector, position of UAV in LTP

^{*} Assistant Professor, Dept. of Mechanical and Astronautical Engineering, MAE/DOV, Senior Member AIAA.

[†] Professor, Dept. of Mechanical and Astronautical Engineering, MAE/KA, Member AIAA.

[‡] Associate Professor, Dept. of Mechanical and Astronautical Engineering, MAE/JO, Senior Member AIAA.

[§] Postdoctoral Researcher, Instituto de Sistemas e Robotica (ISR), Member AIAA.

$\mathbf{p}_c, \hat{\mathbf{p}}_c$	=	vector, position of camera center with respect to target and its estimate
\mathbf{p}_t	=	vector, position of target in LTP
q_c, r_c	=	pitch and yaw rate commands
s	=	tracking loss event
t, τ	=	time
x	=	state vector
y_m	=	camera and altitude measurements
u, v	=	camera measurements
w_y	=	process noise
α	=	rate of tracking loss events
ε	=	the angle between the LOS and the camera heading
γ	=	derivative constant, function of c_ρ
η	=	the angle between \vec{V}_g and $\vec{\lambda}_p$ vectors
ρ	=	horizontal range from the air vehicle to the target
$\bar{\rho}$	=	reciprocal of ρ
ρ_d	=	desired horizontal range to target
ρ_e	=	range error
λ	=	the LOS angle
$\vec{\lambda}_g$	=	the LOS vector
$\vec{\lambda}_p$	=	the vector perpendicular to the LOS
$\lambda_{\min}, \lambda_{\max}$	=	eigenvalues
φ_c, θ_c	=	roll and pitch angles of the camera orientation in inertial frame
ξ	=	state vector of linear system
$\psi, \dot{\psi}$	=	the UAV's heading and turn rate
ψ_h	=	the gimbal pan angle
ψ_t	=	the heading of moving target

I. Introduction

THE past decade has witnessed a remarkable increase in the utilization of unmanned air vehicles (UAVs) both in the US and abroad. This growth is a result of recent advances in communications, solid state sensors, and power supply technologies that have made miniature autopilots and various sensing payloads a reasonable solution for many autonomous applications. Modern UAV applications include a wide variety of intelligence and reconnaissance missions, search and rescue, emergency services, fire scouting, small payload delivery and potentially many others.

While many of the large UAV systems are capable of executing complex missions, their cost is very high and as a result their availability is limited. Consequently there is much interest in the development of small, low-cost platforms which can perform some of the tasks normally assigned to larger UAVs, for example vision-based target

tracking and motion** estimation. This paper addresses the development and flight testing of such a system for a small UAV and extends previous work reported in Ref.1-2.

The complete system consists of a modified remotely controlled (RC) small aircraft equipped with an autopilot and a miniature pan-tilt gimballed camera built using Commercial Off the Shelf (COTS) components (see Fig. 1). In a typical operational scenario when the SUAV is in autonomous flight, the system operator may select a target of interest using a joystick that steers the onboard camera. Once a target is identified by the operator, the image processing algorithm³ computes the target tracking box and provides the position of the centroid of this box in the image frame to the control algorithm. This information is used by an integrated UAV-gimbal control algorithm to steer the UAV and the gimbal to keep the target in the center of the camera frame (i.e. drive the position of the centroid to zero). As is shown in Section II this control strategy results in an orbital motion of the SUAV around the target. In parallel with the control algorithm the centroid position provided by the image processing software is used by a real-time nonlinear filter to obtain estimates of the target motion including position, speed, and heading.

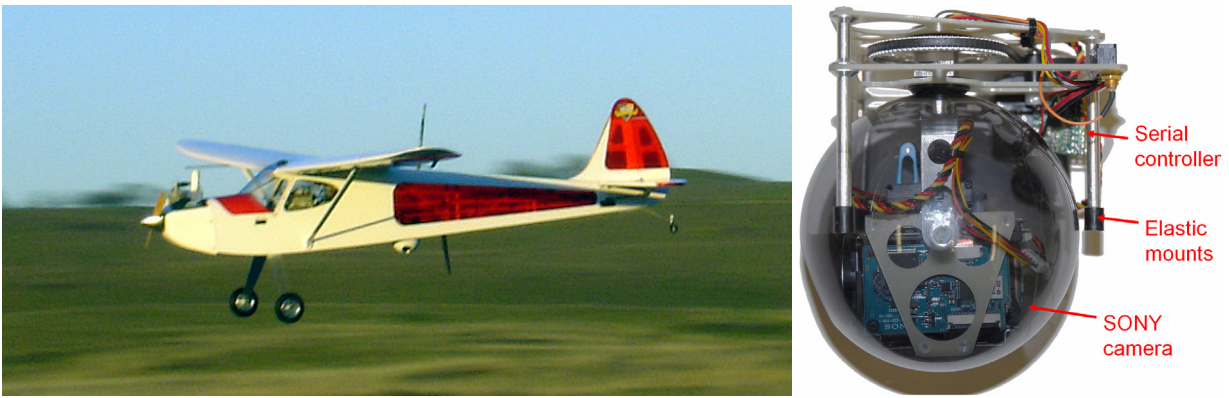


Fig. 1 Modified RC UAV with a gimbaled camera and customized avionics.

Thus this paper addresses two problems. The first one includes the development of a vision-based control algorithm for integrated control of the SUAV and gimbaled camera to maintain the target in the center of the image frame. Since the target position is not known, it is preferable that for feedback this algorithm relies exclusively on the information obtained by the image processing software (centroid position in the camera frame). Ideally, the proposed algorithm should be able to maintain a desired range to the target, although the actual range is not known. The second problem addressed in the paper involves estimating the target position and velocity using the information provided by the image processing software and the onboard GPS and IMU. Estimation of the target

** Term motion refers to position, speed and heading of moving target. It is used here to distinguish the presented results from the algorithms previously published in Ref.1 where only position estimation filter was described.

position is usually referred to in the literature as *target geolocation*, whereas combined position and velocity estimation is known as *target motion estimation*. A critical issue that must be addressed by any vision-based estimation algorithm is the presence of *tracking loss events* defined here as any event that causes the image processing software to lose track of the target.

Vision-based control of robotic manipulators is a mature field as evidenced by an excellent survey paper⁴, where the two most popular approaches to this problem are outlined. In the first approach the control task is defined using the information obtained in the image frame only, while the second approach involves two steps: 1) utilize the image frame information to estimate target position and, possibly, velocity in a global coordinate system and then 2) use these target motion estimates to define a control task. Since estimation introduces lag into the feedback system, avoiding it, if at all possible, makes the first approach preferable.

More recently, the problem of vision-based control and target geolocation has been addressed by the SUAV community, see for example Ref.5-17 and references therein. For vision-based control, the majority of the papers use an existing capability of modern autopilots to establish circular motion with respect to an orbital waypoint (selected by the operator at the proposed target position) at a fixed altitude and radius. During the target localization (the process of estimating target position) a UAV may adjust its flight path by changing the coordinates and radius of the orbital waypoint¹⁵ which is the simplest technique for low altitude and low speed UAVs. For high altitude UAVs, since the target is unlikely to leave the UAV's field of view in a short period of time, there are no time constraints for target localization and therefore coordinated UAV- gimbal control is not considered^{16,17}. Thus, the main focus of these papers is target geolocation.

Target geolocation for airborne applications is done using two approaches. The first one involves finding an intersection of the camera LOS with a local Earth surface¹⁸. This approach is often referred to as a "Geolocation via ray intersection." The second approach¹⁹ employs variations of triangulation for a set of bearing-only-measurements or estimates of distances to the target. Triangulation requires two measurements of the target position in the camera frame. Therefore, the distance between two consecutive measurements (baseline) must be sufficiently large to guarantee low Dilution of Precision (DOP). Clearly, for a small UAV flying around a target, any of the triangulation approaches will result in a large wait-time between the measurements. Moreover, high levels of noise in the LOS attitude measurements amplified by the distance to the target produces errors of the target position estimates that are on the order of 15-25% of the entire LOS length. Therefore, target geolocation from a small UAV flying sufficiently

close can be effectively estimated using triangulation. On the other hand, target geolocation from large distances requires more sophisticated techniques.

Target motion estimation based on image measurements from a fixed-wing UAV has been recently addressed in Ref.15-17. A square-root implementation of the sigma point filter is used in Ref.16-17 to estimate target position and velocity together with a confidence bound for estimation. The confidence bounds for the position estimates are obtained using a priori known noise distributions for all sensors including gimbal angles and camera measurements. The “measurement” of the target is assumed to be constantly at the center of the image frame therefore significantly limiting applicability of the solution. Performance results converge to a 95% confidence interval over a period of 40 and 80 seconds for fixed and moving targets, respectively. However, coordinated control of the UAV and gimballed camera is not considered. Similar research is presented in Ref.15 where the authors consider target localization from the miniature high-wing loading UAV. A simple and elegant solution that uses camera measurements of the target, IMU and GPS and provides a geometric calculation of the LOS intersecting flat ground is proposed. Special emphasis is placed on the analysis of the noise and uncertainty propagation. Interestingly, most of the papers discussed so far do not address a critical issue that always arises in vision-based applications – tracking loss events.

On the other hand, this issue has been addressed extensively in robotics literature. See for example Ref.14 and references therein, where the authors extensively discuss effects of nonhomogeneous illuminations and occlusions on tracking loss events. Traditional methods to deal with occlusions as suggested in Ref.14 are to use multiple cameras or to predict the movement of the target using a track memory containing the history of the previous locations of the target. Another approach reported in Ref.20 includes automatic camera placement that increases the feasible region, circumvents occlusions, and provides uninterrupted tracking. Alternative to pure vision or image processing techniques is a variety of optical flow algorithms^{7,21-23} addressing the task of 3D motion reconstruction from the fast sampled 2D image samples. The computation of optical flow (velocity field) involves several assumptions resulting in numerical issues of differentiation (ill-posed problem), however the framework is initially designed to succeed in the presence of occlusions.

Although a single SUAV is capable of carrying multiple cameras, the techniques reported in robotics literature cannot be easily extended to airborne applications due to highly dynamic UAV-target relative motion. One solution²¹ to this problem consists of employing multiple UAVs that can maintain an uninterrupted view of the target from different locations and angles. Another involves a swarm of micro UAVs deployed from a mother-ship

that can provide imagery of the hidden targets. However, since each approach uses limited throughput wireless communication to deliver compressed video²⁴ and telemetry to the human operator the tracking loss events are unavoidable and must be explicitly addressed. This issue has been central to the design of the particle filter reported in Ref.6. Results show that the particle filter can estimate the target bearing efficiently, even if the image processing algorithm loses track of the target for as many as four consecutive frames.

Previous work by the authors addressed the issue of tracking loss events in Ref.25, 26. In Ref.26 a technique for the design of nonlinear vision-based estimators was proposed and applied to the estimation of a UAV position and velocity with respect to a moving ship. The problem was cast in the LPV framework and the paper provided sufficient conditions for regional stability and performance of the resulting nonlinear estimators. An important feature of the proposed estimators was to complement the vision-based information with the onboard GPS and IMU measurements. The paper suggested dead reckoning as an informal way to deal with tracking loss events, i.e when vision-based measurements are unavailable the estimator integrates GPS/IMU information to provide estimates of the ship position and velocity. These ideas were formalized in Ref.27 where a concept of brief instabilities was introduced (the paper showed that tracking loss events can be modeled as brief instabilities) and sufficient conditions for stability and performance of LPV systems with brief instabilities were given. These conditions were then used to extend the results in Ref.25 to include brief instabilities in the nonlinear estimator design. Furthermore, both works^{25,26} have shown that the lower bound on the estimator performance is related to DOP.

The nonlinear estimator used in this paper to estimate target motion is based on the work previously reported in Ref.25-27. In Ref.27 results obtained in Ref.26 were used to develop a vision-based estimator that complements the onboard Doppler velocity and vision measurements for underwater applications. Furthermore, a small change in the structure of the estimator was introduced that provided better convergence properties. In this paper we apply results of Ref.27 to the estimator proposed in Ref.26 to obtain a nonlinear estimator that integrates vision-based measurements with the information provided by the onboard IMU and GPS to estimate target motion in the presence of tracking loss events. The resulting estimator is extensively tested in simulations, exhibits solid performance in the absence of tracking loss events, and is shown to provide smooth degradation of performance as the duration of tracking loss events increases. These findings are supported by flight test results.

Finally, the paper introduces a novel nonlinear control algorithm for integrated control of the SUAV and the gimbaled camera that maintains a target in the center of the image frame. For feedback, this algorithm relies

exclusively on the information obtained by the image processing software (centroid position in the camera frame), thereby avoiding any lags caused by introducing estimators in the feedback loop. Furthermore, a critical feature of the proposed algorithm is that it can maintain a desired range to target, when the actual range is not known. The paper provides conditions for asymptotic stability of this vision-based system for the case of stationary targets and conditions for ultimate boundedness if the target is moving. The proposed control algorithm is shown to exhibit good performance both in simulation and in flight test.

The paper is organized as follows. The design of the UAV control algorithm is discussed in Section II. The development of the target motion estimator is included in Section III. The systems integration, flight test setup and results of flight experiments with stationary and moving targets are discussed in Section IV. The paper ends with some concluding remarks.

II. Control System Development

Consider Fig. 2, illustrating the horizontal projection of the UAV-target kinematics in the inertial frame $\{I\}$. Let ρ denote horizontal range from the UAV to the target, \vec{V}_g - the UAV ground speed, $\vec{\lambda}_g$ - the LOS vector and $\vec{\lambda}_p$ - the vector perpendicular to $\vec{\lambda}_g$. Furthermore, let ε denote the angle between the LOS vector and the camera centerline (ε represents a target error in frame $\{C\}$ connected to the camera), λ - the LOS angle, ψ - the UAV heading, ψ_h - the gimbal pan angle and η - the angle between the \vec{V}_g and $\vec{\lambda}_p$ vectors. In addition, suppose the target is moving with constant speed V_t , and heading, ψ_t as shown in Fig. 2.

The following set of basic kinematical relations is derived directly from the kinematics of Fig. 2. First, observe that

$$\eta = \psi - (\lambda - \pi/2). \quad (1)$$

Next, projecting the UAV and target speed vectors onto the LOS results in the time derivative of the horizontal range to the target

$$\dot{\rho} = -V_g \sin \eta + V_t \sin(\psi_t - (\psi - \eta)). \quad (2)$$

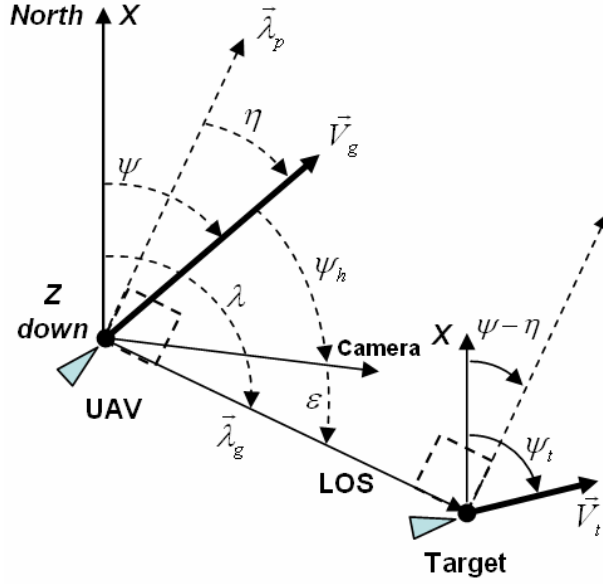


Fig. 2 Moving target tracking for the control law Eq. (2).

Similarly, projecting the same vectors onto the line orthogonal to the LOS produces the rotation speed of the LOS

$$\dot{\lambda} = \frac{V_g \cos \eta}{\rho} - \frac{V_t \cos(\psi_t - (\psi - \eta))}{\rho}. \quad (3)$$

Finally, an expression for the tracking error ε is given by

$$\varepsilon = \lambda - \psi - \psi_h. \quad (4)$$

Substituting Eq. (3) into time derivatives of Eqs. (1) and (4) produces the following set of equations describing the kinematics of the tracking problem

$$\begin{aligned} \dot{\eta} &= -\frac{V_g \cos \eta - V_t \cos(\psi_t - (\psi - \eta))}{\rho} + \dot{\psi} \\ \dot{\varepsilon} &= \frac{V_g \cos \eta - V_t \cos(\psi_t - (\psi - \eta))}{\rho} - \dot{\psi} - \dot{\psi}_h \\ \dot{\rho} &= -V_g \sin \eta + V_t \sin(\psi_t - (\psi - \eta)) \end{aligned} \quad (5)$$

Note that, the two angles η and ε constitute the UAV guidance and gimbal control errors (see Fig. 3). Therefore, the control objective is to drive ε and η to zero using the UAV turn rate $\dot{\psi}$ and gimbal pan rate $\dot{\psi}_h$ as control inputs. This results in the UAV circling around the target while maintaining the target in the center of the image obtained by the camera.

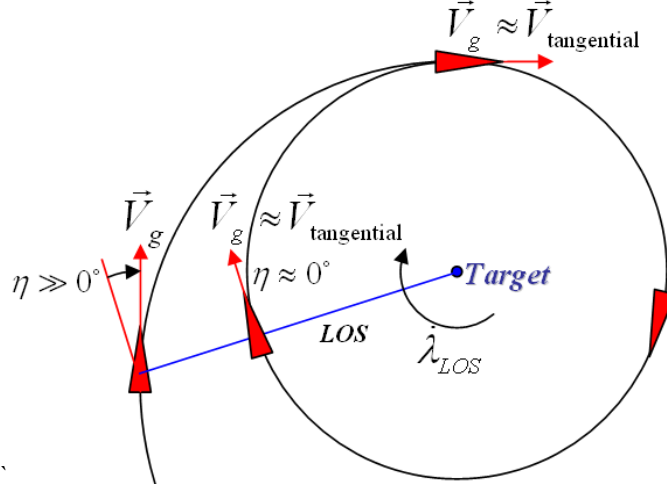


Fig. 3 Illustration of the control strategy.

To achieve this, the following control law is proposed

$$\begin{aligned}\dot{\psi} &= \frac{V_g}{\rho_d} \cos \eta - k_1 \eta, \\ \dot{\psi}_h &= k_1 \eta + k_2 \varepsilon\end{aligned}\quad (6)$$

where ρ_d denotes a desired horizontal range to the target to be selected by the operator, and k_1, k_2 are the feedback coefficients.

Remark 1. The nonlinear control law Eq. (6) includes an interesting feature. As is shown below, it drives the range to the target, ρ , to the desired value ρ_d . This is done for the **unknown** ρ . Intuition suggests that this can be achieved by driving the UAV's yaw rate to the desired value V_g / ρ_d . This emphasizes the fact that the vision-based control law Eq. (6) does not require knowledge of the distance to the target and is thus consistent with the design philosophy discussed in the Introduction: **for feedback use vision only**.

Define $\rho_e = \frac{1}{\rho} - \frac{1}{\rho_d}$, $\bar{\rho} = \rho_e + \frac{1}{\rho_d}$ and $\dot{\rho}_e = -\frac{1}{\rho^2} \dot{\rho}$. Assuming that target heading is constant and can be

arbitrarily chosen, without loss of generality, we chose $\psi_t = 0$; the first equation in Eq. (6) is not affected because the control law is chosen for the turn rate of the UAV. Then it can be shown that the feedback system consisting of Eqs. (5) and (6) is given by:

$$\begin{aligned}
\dot{\eta} &= -V_g \rho_e \cos \eta - k_1 \eta + V_t \cos(\eta - \psi_r) \bar{\rho} \\
\dot{\rho}_e &= \bar{\rho}^2 V_g \sin \eta - V_t \sin(\eta - \psi_r) \bar{\rho}^2, \\
\dot{\varepsilon} &= V_g \rho_e \cos \eta - k_2 \varepsilon - V_t \cos(\eta - \psi_r) \bar{\rho}
\end{aligned} \tag{7}$$

where ψ_r represents relative heading $\psi - \psi_t$ of the UAV with respect to the target.

Note that the system Eq. (7) is a cascaded interconnection of two subsystems

$$\begin{bmatrix} \dot{\eta} \\ \dot{\rho}_e \end{bmatrix} = \begin{bmatrix} -V_g \rho_e \cos \eta - k_1 \eta + V_t \cos(\eta - \psi_r) \bar{\rho} \\ \bar{\rho}^2 V_g \sin \eta - V_t \sin(\eta - \psi_r) \bar{\rho}^2 \end{bmatrix}, \tag{8}$$

and of

$$\dot{\varepsilon} = V_g \rho_e \cos \eta - k_2 \varepsilon - V_t \cos(\eta - \psi_r) \bar{\rho}. \tag{9}$$

For stability analysis, it is convenient to rescale η by introducing a new state variable $\hat{\eta} = \eta / \rho_d$:

$$\dot{x} := \begin{bmatrix} \dot{\hat{\eta}} \\ \dot{\rho}_e \end{bmatrix} = \begin{bmatrix} -V_g \rho_e \cos(\hat{\eta} \rho_d) / \rho_d - k_1 \hat{\eta} + V_t \cos(\hat{\eta} \rho_d - \psi_r) \bar{\rho} / \rho_d \\ \bar{\rho}^2 V_g \sin \hat{\eta} \rho_d - V_t \sin(\hat{\eta} \rho_d - \psi_r) \bar{\rho}^2 \end{bmatrix}, \tag{10}$$

where $x = [\hat{\eta} \ \rho_e]^T$. The following two propositions address stability of the subsystem Eq. (10).

Proposition 1. Consider a linear time-invariant system G :

$$\dot{\xi} = \begin{bmatrix} -k_1 & -V_g / \rho_d \\ V_g / \rho_d & 0 \end{bmatrix} \xi =: A_0 \xi$$

where $V_g \in [V_{g_{\min}}, V_{g_{\max}}]$ and $\rho_d \in [\rho_{d_{\min}}, \rho_{d_{\max}}]$. Then G is globally exponentially stable for any $k_1 > 0$.

Proof. Define a symmetric matrix $P = \begin{bmatrix} \frac{1}{k_1} & \frac{\rho_d}{2V_g} \\ \frac{\rho_d}{2V_g} & \frac{k_1^2 \rho_d^2 + 2V_g^2}{2k_1 V_g^2} \end{bmatrix}$. Then P is positive definite ($P > 0$) for any

$k_1 > 0$ and $A_0^T P + P A_0 = -I$, which completes the proof.

Proposition 2. Define a compact set $\Omega_c = \{\zeta : \zeta^T P \zeta \leq c^2\}$, where the matrix P is given above and

$$c = \frac{c_\rho^2}{\rho_d^2} \lambda_{\min}(P), \quad 0 < c_\rho < 1.$$

i) Suppose $V_t = 0$ and

$$\lambda_{\max}(P) < \frac{\rho_d}{2\gamma V_g} \quad (\text{Condition 1})$$

holds for all constant $V_g \in [V_{g_{\min}}, V_{g_{\max}}]$ and $\rho_d \in [\rho_{d_{\min}}, \rho_{d_{\max}}]$, where $\gamma = c_\rho \sqrt{\left(\frac{c_\rho^2}{4}\right) + \left(2 + c_\rho + \frac{c_\rho}{6}\right)^2}$.

Then origin of (10) is exponentially stable equilibrium for any $x(0) \in \Omega_c$

ii) Suppose, Condition 1 holds and

$$c_\rho - \sqrt{\frac{\lambda_{\max}(P)}{\lambda_{\min}(P)}} \frac{2V_t(1+c_\rho)\sqrt{1+(1+c_\rho)^2}\lambda_{\max}(P)}{\rho_d - 2\gamma V_g \lambda_{\max}(P)}} > 0 \quad (\text{Condition 2})$$

is valid for all $V_t : \sup_{t \geq 0} |V_t(t)| \leq V_{t_{\max}}$, $V_g \in [V_{g_{\min}}, V_{g_{\max}}]$ and $\rho_d \in [\rho_{d_{\min}}, \rho_{d_{\max}}]$.

Then system Eq. (10) is ultimately bounded for any $x(0) \in \Omega_c$

Proof. See Appendix.

Remark 2. Since $\hat{\eta} = \eta/\rho_d$ we conclude that stability and ultimate boundedness of the system Eq. (10) imply stability and ultimate boundedness of feedback system Eq. (8).

Remark 3. Consider system Eq. (9): $\dot{\varepsilon} = V_g \rho_e \cos \eta - k_2 \varepsilon - V_t \cos(\eta - \psi_r) \bar{\rho}$. Notice that the homogeneous system $\dot{\varepsilon} = -k_2 \varepsilon$ is globally uniformly exponentially stable and therefore Eq. (9) is ‘‘Bounded Input Bounded Output’’ stable. Suppose $V_t = 0$. Then it²⁸ follows from Proposition 2 that $V_g \rho_e \cos \eta \rightarrow 0$ and therefore $\varepsilon \rightarrow 0$.

On the other hand, if $V_t \neq 0$ the term $\frac{V_t}{\rho_d} \cos(\eta - \psi_r) \bar{\rho}$ in Eq. (5) is bounded in Ω_c and therefore so is ε .

Remark 4. We notice that Condition 1 guarantees that $\rho_d - 2\gamma V_g \cdot \lambda_{\max}(P) > 0$ for all constant $V_g \in [V_{g_{\min}}, V_{g_{\max}}]$ and $\rho_d \in [\rho_{d_{\min}}, \rho_{d_{\max}}]$. Therefore, Condition 2 can always be satisfied for sufficiently small V_t .

Remark 5. Conditions 1 and 2 are used to select an appropriate value for the gain k_1 as illustrated in Fig. 4 for the

cases of stationary and moving targets. Let $e_1 = \lambda_{\max}(P) - \frac{\rho_d}{2\gamma V_g}$ and

$$e_2 = c_\rho - \sqrt{\frac{\lambda_{\max}(P)}{\lambda_{\min}(P)}} \cdot \frac{2V_i(1+c_\rho)\sqrt{1+(1+c_\rho)^2}\lambda_{\max}(P)}{\rho_d - 2\gamma V_g \lambda_{\max}(P)}. \quad \text{Figures 4a-4b correspond to the case of a}$$

stationary target, where Fig. 4a includes a 3D plot of e_1 vs. k_1 and c_ρ for typical values of

$V_g = 25 \text{ m/s}$ and $\rho_d = 200 \text{ m}$. Figure 4b shows the intersection of the plain $e_1 = 10^{-4}$ with the 3D surface

shown in Fig. 4a for increasing values of ρ_d ($V_g = 25 \text{ m/s}$). These intersections result in a family of 2D graphs

of k_1 vs. c_ρ . (We observe that c_ρ represents the size of the RA. For example, if $c_\rho = 0.1$ then exponential

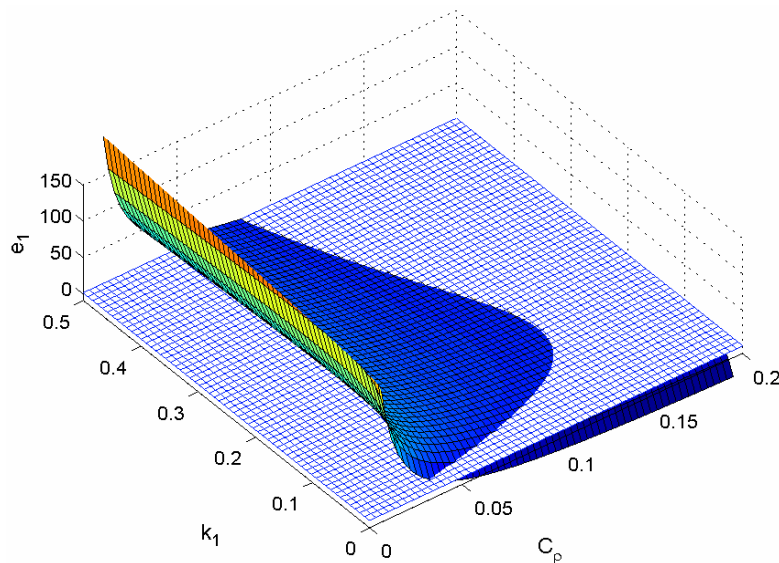
convergence to the origin is guaranteed for initial values $|\eta(0)| < 0.1 \text{ rad}$ and $0.9\rho_d \leq \rho(0) \leq 1.1\rho_d$). Clearly,

$e_1 = 10^{-4}$ implies that Condition 1 is satisfied for $c_\rho \leq 0.14$ at the selected nominal flight condition and for a

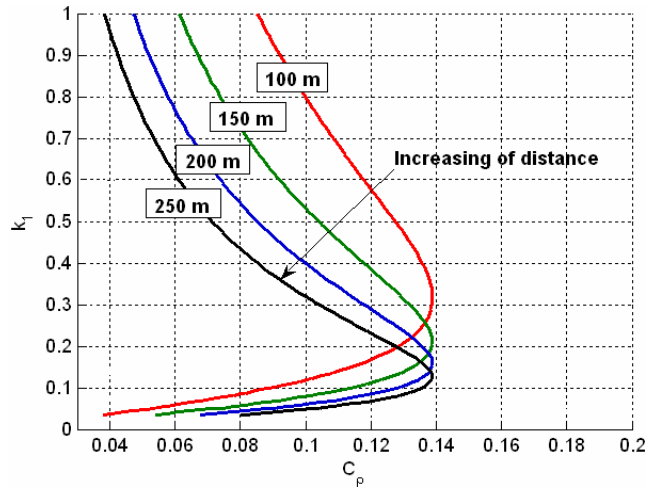
range of values of the gain k_1 . Furthermore, Condition 1 illustrated in Fig. 4a provides an optimal choice of k_1 that

maximizes the size of the RA. For example, for $\rho_d = 200 \text{ m}$ and maximum c_ρ the best choice of feedback gain

is $k_1 = 0.15$.

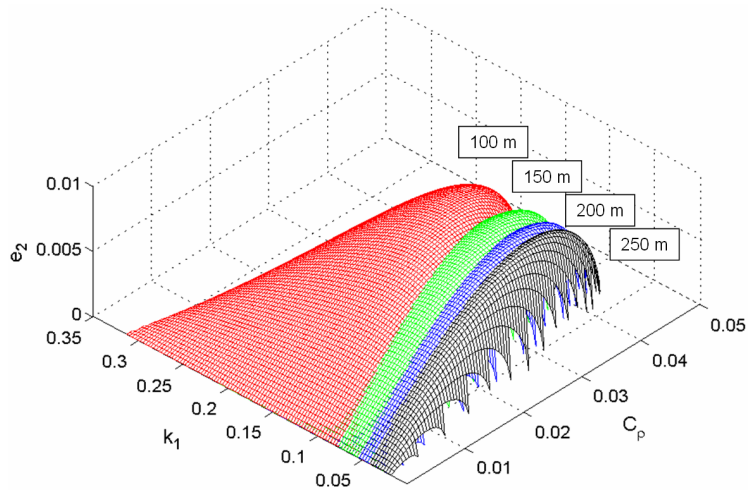


a) Fixed target, $e_1 = f(k_1, c_\rho)$.



b) Fixed target, variation of ρ_d .

c) Moving target, $e_2 = f(k_1, c_p)$.



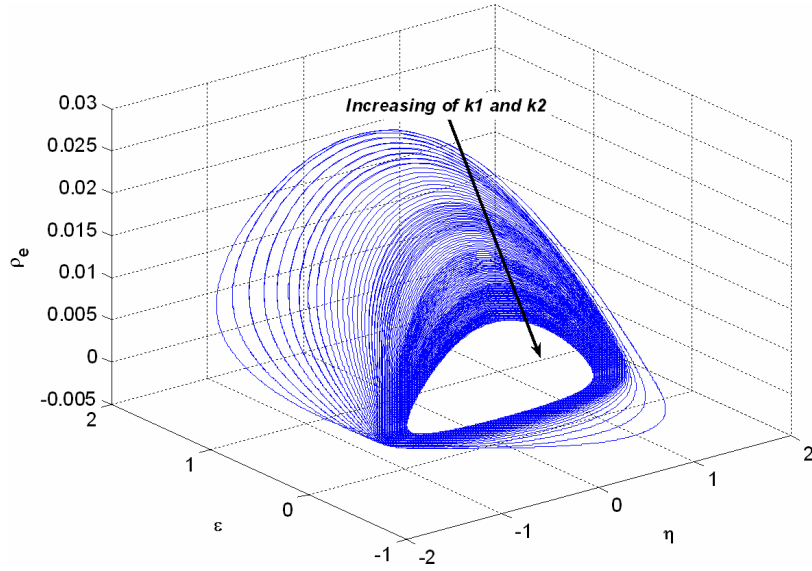
d) Moving target, variation of ρ_d .

Fig. 4 Stability regions for fixed and moving targets.

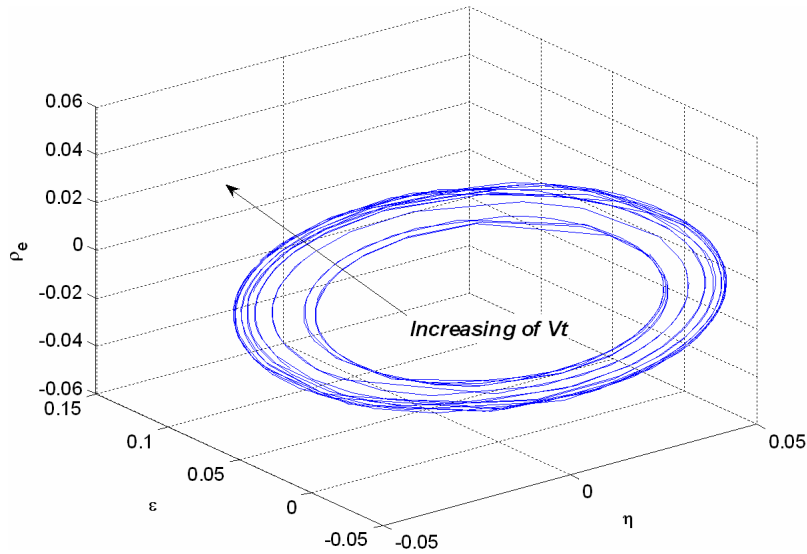
The case of the moving target (Condition 2) is illustrated in Fig. 4c-4d. Figure 4c includes a 3D plot of e_2 vs. k_1 and c_ρ for the same values of V_g and ρ_d as above and for target moving with speed $V_t = 1m/s$. Analysis of the size of the RA characterized by the range of c_ρ shows that it is significantly smaller (an order of magnitude) when the target is moving, which is expected. The impact of ρ_d on the size of the RA is almost identical to the case of a stationary target (see Fig.4a) except for the fact that the maximum c_ρ is about 0.04 (vs. 0.14 for the fixed target). The dependence of the size of RA on ρ_d is illustrated in Fig.4c, where the 3D surfaces in Fig. 4d are plotted for different values of ρ_d . This analysis shows that the gain k_1 must increase as the range to the target decreases. This observation is rooted in the kinematics of the problem: the turn rate of the LOS is bounded by $[|V_t - V_g|/\rho_d, |V_t + V_g|/\rho_d]$ and is therefore inversely proportional to ρ_d . Since V_t is unknown, the greater values of k_1 are required to achieve the necessary turn rate (see Eq. (6)). Finally, we note that this numerical analysis resulted in $V_{t_{\max}} = 2.5m/s$. This value is conservative as is shown in simulation results below (Fig. 7).

Next, plots of the steady state trajectories of the entire nonlinear system Eq. (7) in response to a number of initial conditions are included in Fig.5. The impact of increasing the gains k_1 , k_2 for a fixed V_t on the trajectories of the feedback system Eq. (7) is illustrated in Fig.5a. In turn, the influence of increasing V_t for fixed k_1 and k_2 is demonstrated in Fig.5b. The figures show that the navigation and target tracking errors of the feedback system Eq. (7) are proportional to V_t and inversely proportional to k_1 and k_2 .

The control system architecture implementing control law Eq. (6) is presented in Fig. 6. It consists of an autopilot and a gimbal driven by the control inputs $\dot{\psi}$ and $\dot{\psi}_h$. The onboard camera provides real-time video to the image tracking software³. This software, when target lock is engaged, computes the tracking error, ε , while the onboard GPS and inertial systems provide a solution for the navigation error, η .



a) Impact of increasing k_1, k_2 .



b) Impact of increasing V_t .

Fig. 5. Steady state trajectories.

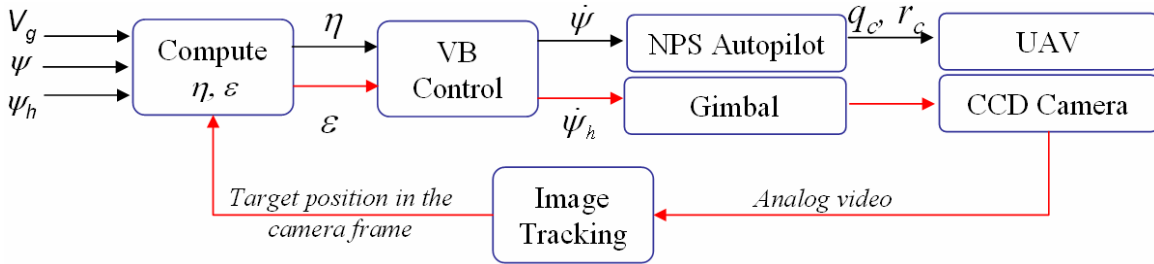


Fig. 6. Control system architecture.

Results of a 6DOF nonlinear simulation (Fig.7) of target tracking for two different target speeds show that the control law performs remarkably well when tracking a moving target while using information obtained from the onboard camera and the UAV velocity available from the onboard GPS. The second subplot (Fig.7b) shows the dynamics of the range to the tracking object when the UAV is orbiting the target; this demonstrates the effectiveness of the designed control law. Analysis shows that the higher the UAV speed over the speed of the target the more effective the range holding capability is.

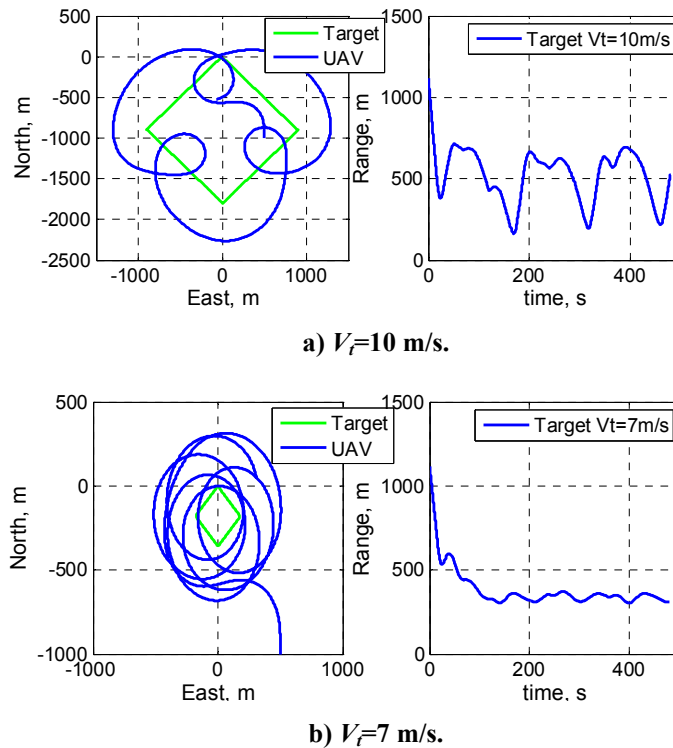


Fig. 7 UAV motion versus target motion.

The results above are obtained for continuous tracking conditions and, therefore, do not include the effect of target loss events. In the presence of tracking loss events, the control system uses the latest estimates of target position and velocity provided by the target motion estimator to continuously compute the UAV turn rate and gimbal control commands. A target motion estimator that is robust in the presence of target loss events is discussed next.

III. Target Motion Estimation

In this paper we assume that the UAV's altitude above the target is known, and we use it as an additional measurement. To obtain this measurement we use the filter developed in Ref. 1 to get the target latitude and

longitude. The target altitude is then obtained in real-time from a geo-referenced database made available from the Perspective View Nascent Technologies (PVNT) software package²⁹ by providing it with the estimated target latitude and longitude. The key contribution of this paper is to obtain a precise estimate of target velocity by integrating the filtering solution provided in Ref. 1, PVNT altitude estimates and a nonlinear estimator that integrates vision and onboard GPS velocity measurements, which is discussed next.

Consider Fig.8, which depicts an aircraft equipped with a gimbaled camera pointing at a moving target. Let $\{I\}$ denote an inertial reference frame, $\{B\}$ a body-fixed frame that moves with the UAV, and $\{C\}$ a gimbaled-camera frame that is attached to the origin of $\{B\}$ but rotates with respect to $\{B\}$.

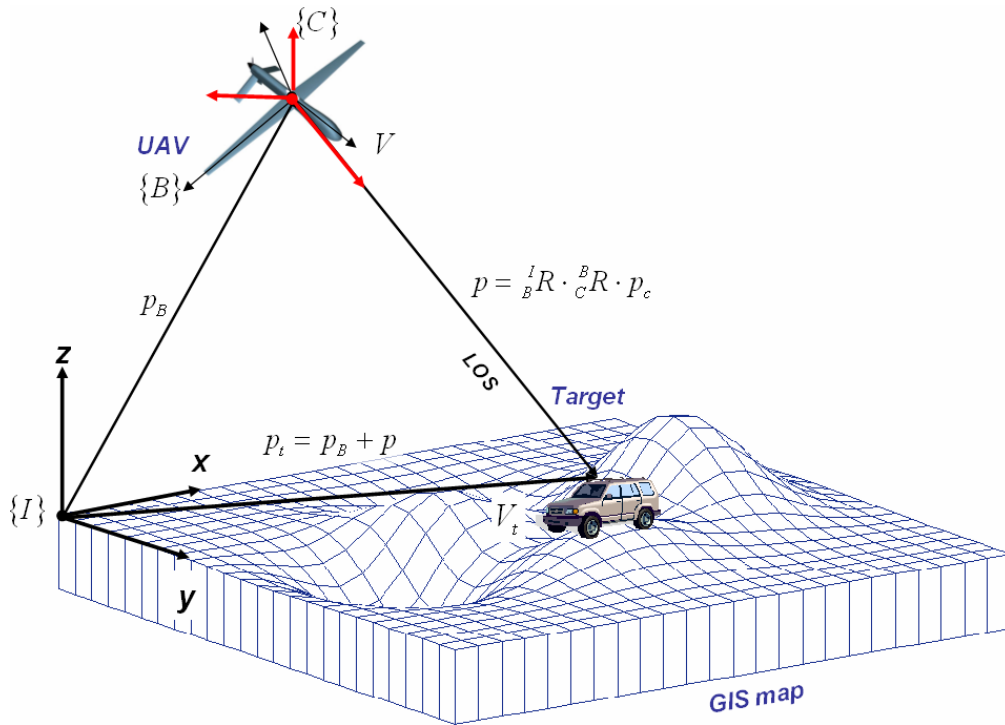


Fig. 8. UAV-Target relative kinematics

Suppose that the target inertial velocity, V_t , and heading, ψ_t , are constant. Following the notation introduced in Ref. 25, let $\mathbf{p}_c = [x_c \ y_c \ z_c]^T$ denote the relative position of the center of $\{C\}$ with respect to the target resolved in $\{C\}$ and let ${}^I R$ denote the coordinate transformation from $\{C\}$ to $\{I\}$ as ${}^I R = {}^I R \cdot {}^B R \cdot {}^C R$. The transformation ${}^B R$ is computed onboard the UAV using known pan and tilt angles provided by the gimbal, and ${}^I R$ is calculated using roll, pitch and yaw angles of the UAV provided by the autopilot.

The expression for measurements provided by the image processing software is obtained using a simple pinhole camera model with an assumption of fixed zoom and known camera geometry

$$\begin{bmatrix} u \\ v \end{bmatrix} = \frac{f}{x_c} \begin{bmatrix} y_c \\ z_c \end{bmatrix}, \quad (11)$$

where f is the focal length of the camera and $[u \ v]^T$ are the coordinates of the centroid of the target image in $\{C\}$. These measurements are provided by the image tracking software when target lock is engaged. Since the camera onboard is gimbaled, the target is always located in front of the camera image plane, i.e. $x_c > 0$. As discussed above in addition to measurements in Eq. (11) we use the UAV altitude above the target:

$$z = -x_c \sin \theta_c + y_c \sin \varphi_c \cos \theta_c + z_c \cos \varphi_c \cos \theta_c, \quad (12)$$

where φ_c , θ_c represent the total roll and pitch angles that determine orientation of $\{C\}$ with respect to $\{I\}$. Define

$$\mathbf{g}_{\varphi\theta}(\mathbf{p}_c) = \begin{bmatrix} \frac{f}{x_c} y_c \\ \frac{f}{x_c} z_c \\ -x_c \sin \theta_c + y_c \sin \varphi_c \cos \theta_c + z_c \cos \varphi_c \cos \theta_c \end{bmatrix}. \quad (13)$$

Then the process model considered in this paper has the following form

$$\begin{cases} \frac{d}{dt} \mathbf{p} = -\mathbf{V} + \mathbf{V}_t \\ \frac{d}{dt} \mathbf{V}_t = 0 \\ \mathbf{y} = \mathbf{g}_{\varphi\theta}(\mathbf{p}_c), \mathbf{p}_c = {}^I R \cdot \mathbf{p} \end{cases}, \quad (14)$$

where \mathbf{p} is position of the target w/r to the UAV, $\mathbf{y} = [u \ v \ z]^T$ denotes ideal camera and altitude measurements, \mathbf{V} is the inertial velocity of the UAV and the target velocity, \mathbf{V}_t , $(\|\mathbf{V}_t\| \leq V_{t_{\max}})$ is assumed to be constant.

The practical problem now consists of determining the relative position and velocity of the moving target with respect to the UAV using IMU, GPS and camera measurements complemented by the altitude above the target provided in real-time by the PVNT system²⁹. During numerous flight tests¹ the image tracking software (Section V)

lost track of the target on a regular basis primarily due to the dynamic change of lighting conditions and radio frequency interference in video and control links. This prompted the following question: can the filtering solution maintain stability in the presence of tracking loss events? In fact, the ideas presented in Ref. 25- 27 are used in this paper to derive a nonlinear filter that provides estimates of target motion using the process model Eq. (14) in the presence of such events.

Following the development in Ref. 26, define a tracking loss as a binary signal $s: [0, \infty) \rightarrow \{0, 1\}$

$$s = s(t) = \begin{cases} 0 & \text{tracking loss event at time } t \\ 1 & \text{camera tracks the target at time } t \end{cases}.$$

For a given binary signal s and $t > \tau > 0$, let $T_s(\tau, t)$ denote the length of time in the interval (τ, t) that $s = 0$.

Then formally

$$T_s(\tau, t) := \int_{\tau}^t (1 - s(l)) dl.$$

The signal, s , is said to have brief tracking loss events if $T_s(\tau, t) \leq T_0 + \alpha(t - \tau)$, $\forall t \geq \tau \geq 0$, for some $T_0 \geq 0$

and $\alpha \in [0, 1]$. Note, that α represents an upper bound on the ratio $\frac{T_s(\tau, t) - T_0}{t - \tau}$, i.e the total time the target is lost

on a given interval as a fraction of the interval duration.

The nonlinear estimator used in this paper is given next (see also Fig. 7.)

$$\begin{cases} \frac{d}{dt}(\hat{\mathbf{p}}) = -\mathbf{V} + \hat{\mathbf{V}}_t + s \cdot K_1 \cdot {}^I R \cdot H^{-1}(\hat{\mathbf{p}}_c) \cdot (\mathbf{g}_{\varphi\theta}(\hat{\mathbf{p}}_c) - \mathbf{y}_m) \\ \frac{d}{dt} \hat{\mathbf{V}}_t = s \cdot K_2 \cdot {}^I R \cdot H^{-1}(\hat{\mathbf{p}}_c) \cdot (\mathbf{g}_{\varphi\theta}(\hat{\mathbf{p}}_c) - \mathbf{y}_m) \\ \hat{\mathbf{p}}_c = {}^C R \cdot \hat{\mathbf{p}} \end{cases}, \quad (15)$$

where $H(\mathbf{p}_c)$ is the Jacobian of the nonlinear transformation $\mathbf{g}_{\varphi\theta}(\mathbf{p}_c)$:

$$H(p_c) = \begin{bmatrix} -\frac{f y_c}{x_c^2} & \frac{f}{x_c} & 0 \\ -\frac{f z_c}{x_c^2} & 0 & \frac{f}{x_c} \\ -\sin \theta_c & \cos \theta_c \sin \varphi_c & \cos \theta_c \cos \varphi_c \end{bmatrix}. \quad (16)$$

and \mathbf{y}_m represents the noisy measurements of \mathbf{y} . It is easy to check that $\det(H) = f^2 z_c / x_c^3$ and therefore $H(\mathbf{p}_c)$ is always invertible for all admissible values of \mathbf{p}_c , φ_c , θ_c except at the relative altitude $z_c=0$.

The estimation solution Eq. (15) extends results proposed in Ref. 27 to include tracking loss events. Theorems 1 and 2 in Ref. 26 were used to obtain the gains K_1 , K_2 that guarantee regional stability and performance of the estimator Eq. (15) in the presence of brief tracking loss events characterized by the parameters T_0 and α . In fact, in Ref. 26 it is shown that the best achievable performance of the filter Eq. (15) is bounded below by a DOP-like quantity $\gamma = f(T_0, \alpha) \max_{p_c \in P_c} \left\| \left(H^T(p_c) H(p_c) \right)^{-1} \right\|$, where P_c represents a bounded set of all the allowable values of the vector p_c and the function $f(T_0, \alpha)$ is proportional to T_0 and α (recall, T_0 and α characterize the duration of tracking loss events). In fact, as α approaches 1, $f(T_0, \alpha)$ goes to infinity. Therefore, as the Jacobian matrix H becomes ill conditioned (due to poor geometry) the lower bound on the achievable performance goes to infinity. The same is true for longer duration of the tracking loss events. Indeed, as α approaches 1 – no tracking – γ blows up.

Implementation of the estimator Eq. (15) is shown in Fig.9. When the tracking loss event occurs, the estimator integrates the UAV velocity measurements to obtain an estimate of the relative position (dead reckoning). When target tracking is reestablished the integrators are reinitialized based on the real-time vision-based measurements, y_m , provided through the feedback.

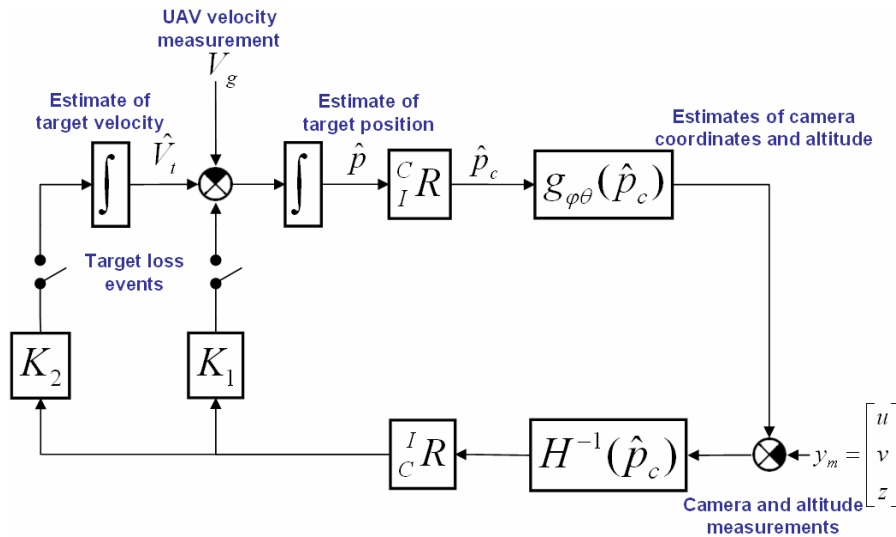


Fig. 9. Implementation of estimator Eq. (12).

Next, the entire system including the control law Eq. (6) and the estimator Eq. (15) was tested in a full scale 6DOF nonlinear simulation in the presence of measurement noise and modeled wind (Dryden Wind Turbulence Model). The scenario used in the simulation (Fig.10) assumed identification of a moving target and a start of target tracking at 2.5 s after the beginning of the flight. This is followed by initialization of the position estimation filters at 26 s when the object of interest was at 50° starboard. Between 2.5 s and 26 s, the UAV experiences transient of the control law that brings the UAV to an orbital motion around the moving target. The target is moving with a constant ground speed of 14 m/s and heading 45°. Based on the analysis of measurements from numerous flight experiments with the Piccolo autopilot³⁰, the following sensor noise were applied to the simulation: IMU noise for each channel with 0° mean and 0.2° variance, camera noise for both channels with 0° mean and 2.5° variance, measurements of altitude above the target with 0m mean and 20m variance. (Here we assumed the worst case scenario only when GPS measurements are available and the target is moving on flat ground at a known altitude).

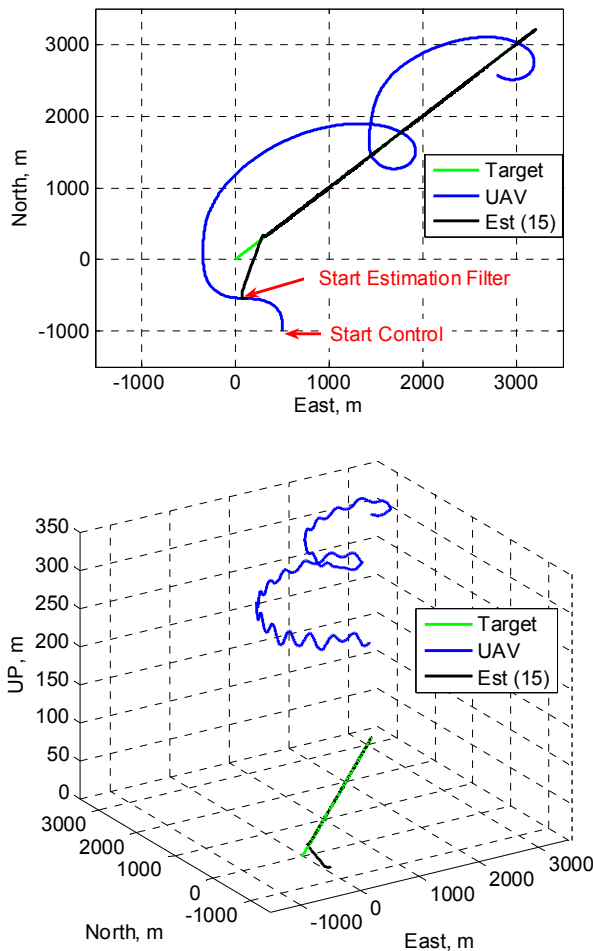


Fig. 10 3D and 2D projections of relative motion.

The results of this simulation for the ideal case when no tracking loss events occur ($\alpha = 0$) are presented next. Figure 10 shows plane and 3D projections of the target, UAV trajectories and the projection of the estimated target position obtained with estimator Eq. (15). The filter is initialized with the horizontal coordinates of the UAV but with the altitude of the target. Analysis shows that except for the very short convergence interval the estimated target position closely follows the true motion of the target. Figure 11 represents the filtering results for position, speed and heading estimation errors. It can be seen that in an ideal scenario with $\alpha = 0$ the convergence time for the positional error (see Fig.11.a – shows convergence to 10 m) does not exceed 5.5 s and 11 s for both speed and heading (see Fig.11.b – shows convergence to 5 m/s and 5°).

Analysis of the same experiment with a variable tracking loss parameter α is presented next in Fig.12. Speed of convergence was the metric used to evaluate the performance of the filter as α increases. Specifically, this was defined to be the 1st time instant past which the estimate stays within 10% of the true value. Here P_{conv} represents the position metric and V_{conv} – the velocity metric.

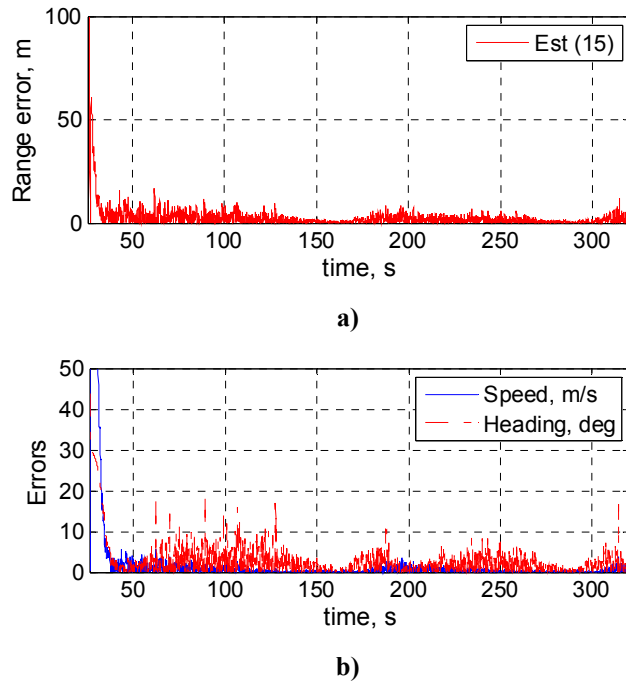


Fig. 11 Convergence results for filter Eq. (15): position, velocity and heading errors.

The analysis shows that the filter exhibits stable convergence times for both position and velocity estimates in the presence of tracking loss events characterized by α as high as 0.45 (the target is lost 45% of the time). The target position estimator (TPE) convergence time, P_{conv} , for the nonlinear filter reported earlier in Ref. 1 is also included in Fig. 12 for comparison purposes. In fact, TPE is a Kalman filter with values of the gains obtained for a

specific set of horizontal distances to the target. Filter Eq. (15) outperforms the TPE for the entire range of values of α considered, as illustrated in Fig.12.

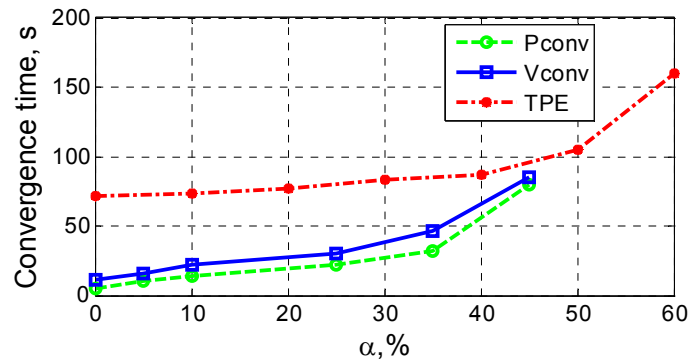


Fig. 12 Convergence time vs. variable α %.

IV. Flight Test Results

The flight test setup to test the filter Eq. (15) is almost identical to the one described earlier in Ref. 1 and is shown in Fig.13. A customized low cost RC model aircraft (see Fig.1) was used to house the gimbaled camera, wireless video and serial links as well as the Piccolo Plus autopilot³⁰ with its dedicated 900 Mhz control link.

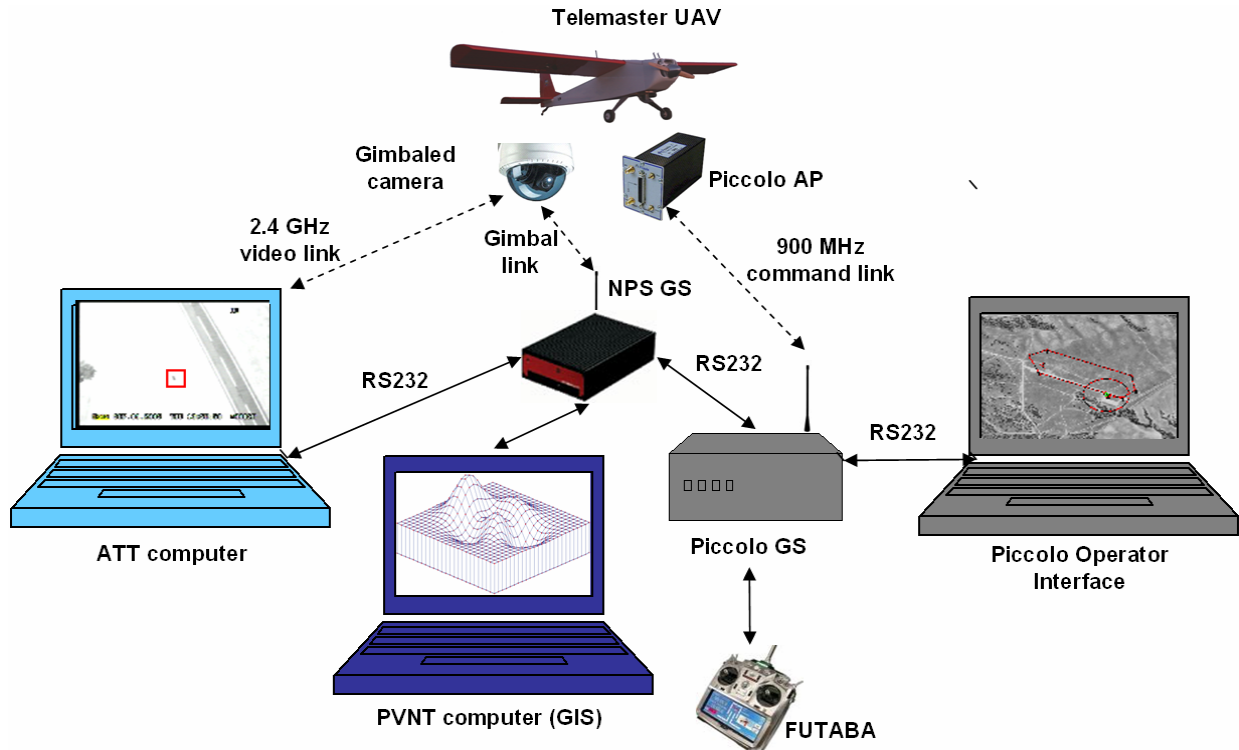


Fig. 13 Flight test setup.

A low-cost PTZ gimbal was designed and manufactured around an inexpensive black-and-white CCTV camera. The 330g servo-based unit provides $\pm 180^\circ$ pan and $0-90^\circ$ tilt operation, with better than 10 bit resolution and speeds of 200 deg/sec in pan, and 600 deg/sec in tilt. All airborne hardware, including the AP cost less than \$10K. The image obtained by the onboard camera was broadcast on a 2.4 GHz analog link and processed on the ground by the off-the-shelf PerceptiVU image processing software³.

PerceptiVU allows the user to select and lock on a target displayed on a ground station screen. In the configuration used in this experiment, PerceptiVU provides coordinates of the centroid of the target selected by the user with an update rate of 30 Hz. These coordinates were then employed by the control and filtering algorithms introduced in previous sections that were implemented on the NPS ground control station (GCS).

Multiple flight tests of the complete system were conducted. During the tests the target (white minivan) was moving along the side of the runway with a fixed speed of 4-5 m/s and heading 296° (parallel to the runway). When the tracking lock was manually engaged the target was framed by the red tracking gate (color-coded for intuitive interaction with human operator), the coordinates of the center of the gate were then sent to the NPS GCS (see a sequence of frames in Fig.14). In order to evaluate the system performance the position, direction and speed of the target were continuously measured by a GPS receiver.



Fig. 14 An example of visual tracking.

Results of tracking and motion estimation are summarized in Fig.15. For the sake of comparison they also represent implementation of two estimation algorithms; an original TPE filter reported in Ref. 1 and a motion estimation (TME) filter Eq. (15). Figure 15 includes a 3D plot of the UAV trajectory (at the top) as well as the estimates of the target position (at the bottom). The UAV trajectory is color coded to display the time intervals where the target track was lost. Due to the low speed of the target, the control law maintains a circular motion with the turn radius of about 200m and a slowly moving center as predicted by the analysis presented in Section II.

Range estimation errors are shown in Fig.16, velocity estimation errors of TME filter are shown in Fig.17. Superimposed on the position estimation error plot is the time history of the tracking loss events; tracking is enabled when the signal is at high level and the track is lost when it is at zero.

As can be seen from Fig. 16, the TME filter Eq. (15) performs significantly better than the TPE filter¹, while the velocity estimation error obtained with the filter Eq. (15) does not exceed 0.5 m/s.

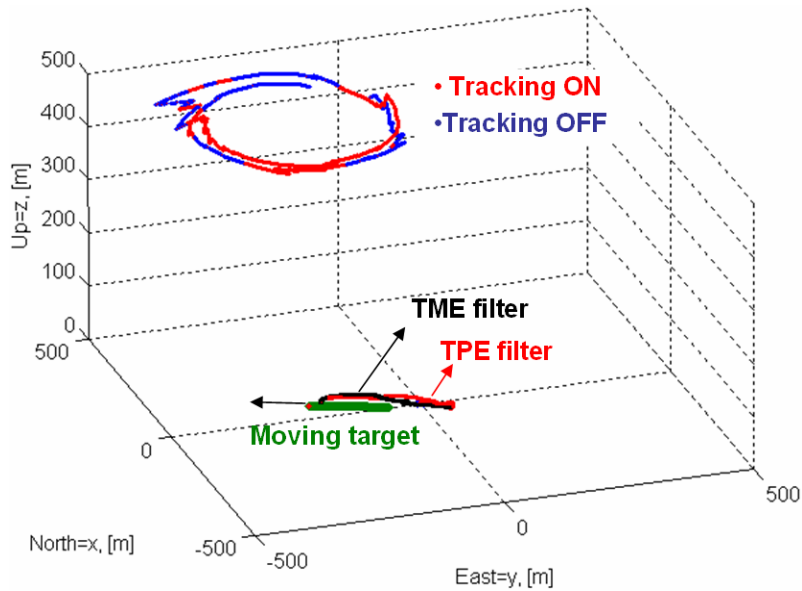


Fig. 15 Flight test result of tracking a moving target.

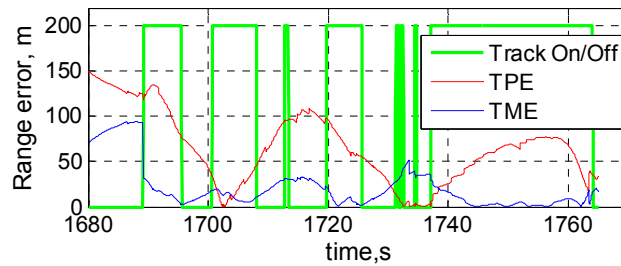


Fig. 16 Flight test range estimation errors for two algorithms.

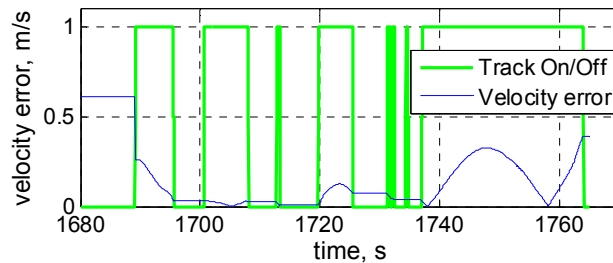


Fig. 17 Flight test velocity estimation error.

V. Conclusions

A system capable of tracking a moving target and estimating its position and velocity was developed. Straightforward nonlinear analysis was used to motivate a simple control system for coordinated control of a UAV and of gimbaled camera. An interesting aspect of this algorithm is that for feedback it relies on the information obtained from the onboard camera directly, thereby eliminating any lags caused by introducing an estimator in the feedback loop. In addition, a critical feature of the proposed algorithm is that it can maintain a desired range to target, when actual range is not known. Results of the stability analysis for both stationary and moving target cases provided explicit means of choosing the control gains.

Furthermore, a nonlinear filter for target motion estimation was introduced. The filter performance was analyzed in the presence of tracking loss events. It was shown that the filter exhibited graceful degradation of performance in the presence of these events. The extensive results of multiple flight test for moving targets supported this conclusion.

Having been implemented onboard a low cost (< \$10K) generic UAV system and tested in numerous flight experiments the entire system shows remarkable robustness to unpredictable flight conditions and human operator related factors. Overall, the control system and target motion estimator were shown to perform well in both nonlinear simulation and in numerous flight tests.

Future work will address improving performance of the target tracking and motion estimation algorithms by decreasing convergence times, reducing occurrence of tracking loss events and minimizing their impact on the filter performance.

Appendix

Proof of **Proposition 2**: Define a candidate Lyapunov function $V = x^T Px$ and consider the system

$$\dot{x} = A_0 x + \Delta f(x) \tag{A1}$$

where $\Delta f(x) = f(x) - A_0 x$. Clearly Eq. (A1) is equivalent to Eq. (10). Then

$$\dot{V} = \frac{d}{dt}(x^T Px) = -x^T x + 2\Delta f^T(x)Px \tag{A2}$$

where

$$\Delta f(x) = \begin{bmatrix} V_g \rho_e (1 - \cos \hat{\eta} \rho_d) / \rho_d + V_t \bar{\rho} \cos(\hat{\eta} \rho_d - \psi_r) / \rho_d \\ V_g \bar{\rho}^2 \sin \hat{\eta} \rho_d - V_t \bar{\rho}^2 \sin(\hat{\eta} \rho_d - \psi_r) - \frac{V_g}{\rho_d} \hat{\eta} \end{bmatrix} \quad (\text{A3})$$

Since $\lambda_{\min}(P) \|x\|^2 \leq x^T P x \leq \lambda_{\max}(P) \|x\|^2$ we obtain that in $x \in \Omega_c \Rightarrow \|x\| \leq \frac{c_\rho}{\rho_d}$, and thus

$$|\rho_e| = \left| \frac{1}{\rho} - \frac{1}{\rho_d} \right| \leq \frac{c_\rho}{\rho_d} \Rightarrow \frac{(1 - c_\rho)^2}{\rho_d^2} \leq \bar{\rho}^2 \leq \frac{(1 + c_\rho)^2}{\rho_d^2}, \quad \forall x \in \Omega_c, \quad (\text{A4})$$

Set $V_t = 0$ in Eq. (A3). By applying the identity $1 - \cos \eta = 2 \cdot \sin^2 \frac{\eta}{2}$ to $\Delta f(x)$ we obtain that

$$\Delta f(x) = \begin{bmatrix} V_g \rho_e (1 - \cos \hat{\eta} \rho_d) / \rho_d \\ V_g \bar{\rho}^2 \sin \hat{\eta} \rho_d - \frac{V_g}{\rho_d} \hat{\eta} \end{bmatrix} = \frac{V_g}{\rho_d^2} \begin{bmatrix} 2 \cdot \rho_d \rho_e \sin^2 \frac{\eta}{2} \\ \rho_d^2 \bar{\rho}^2 \sin \eta - \eta \end{bmatrix}. \quad (\text{A5})$$

Then

$$\|\Delta f(x)\|^2 = \left(\frac{V_g}{\rho_d^2} \right)^2 \left(\left(2 \rho_d \rho_e \sin^2 \frac{\eta}{2} \right)^2 + \left(\rho_d^2 \bar{\rho}^2 \sin \eta - \eta \right)^2 \right). \quad (\text{A7})$$

By applying Eq. (A4) to $\|\Delta f(x)\|^2$ we obtain the following upper bound

$$\begin{aligned} \|\Delta f(x)\|^2 &\leq \left(\frac{V_g}{\rho_d^2} \right)^2 \left(4c_\rho^2 \left(\frac{\eta^2}{4} \right)^2 + \left((1 + c_\rho) \sin \eta - \eta \right)^2 \right) = \left(\frac{V_g}{\rho_d^2} \right)^2 \left(c_\rho^2 \left(\frac{\eta^2}{2} \right)^2 + (c_\rho (2 + c_\rho) \sin \eta + \sin \eta - \eta)^2 \right) \\ &\leq \left(\frac{V_g}{\rho_d^2} \right)^2 \left(c_\rho^2 \left(\frac{\eta^2}{2} \right)^2 + (c_\rho (2 + c_\rho) |\eta| + |\sin \eta - \eta|)^2 \right), \quad \forall x \in \Omega_c \end{aligned} \quad (\text{A8})$$

It follows from Lemma 1 in Ref. 31 that $|\sin \eta - \eta| \leq |\eta|^3 / 6$. Using this bound we obtain that

$$\begin{aligned} \|\Delta f(x)\|^2 &\leq \left(\frac{V_g}{\rho_d^2} \right)^2 \left(c_\rho^2 \left(\frac{\eta^2}{2} \right)^2 + \left(c_\rho (2 + c_\rho) |\eta| + \frac{|\eta|^3}{6} \right)^2 \right) \leq \left(\frac{V_g}{\rho_d^2} \right)^2 \left(c_\rho^2 \left(\frac{c_\rho^2}{4} \right) \eta^2 + c_\rho^2 \left((2 + c_\rho) |\eta| + \frac{c_\rho}{6} |\eta| \right)^2 \right) \\ &\leq \left(\frac{V_g}{\rho_d^2} \right)^2 \left(c_\rho^2 \left(\frac{c_\rho^2}{4} \right) + c_\rho^2 \left((2 + c_\rho) + \frac{c_\rho}{6} \right)^2 \right) \eta^2 = c_\rho^2 \left(\frac{V_g}{\rho_d} \right)^2 \left(\left(\frac{c_\rho^2}{4} \right) + \left(2 + c_\rho + \frac{c_\rho}{6} \right)^2 \right) \hat{\eta}^2, \quad \forall x \in \Omega_c \end{aligned} \quad (\text{A9})$$

where we used the fact that $x \in \Omega_c \Rightarrow |\hat{\eta}| \leq \frac{c_\rho}{\rho_d} \Rightarrow |\eta| \leq c_\rho$. Using Eq. (A9) we derive an upper bound

on $\|\Delta f(x)\|$:

$$\begin{aligned} \|\Delta f(x)\| &\leq c_\rho \left(\frac{V_g}{\rho_d} \right) \sqrt{\left(\frac{c_\rho^2}{4} \right) + \left(2 + c_\rho + \frac{c_\rho}{6} \right)^2} |\hat{\eta}| \leq c_\rho \left(\frac{V_g}{\rho_d} \right) \sqrt{\left(\frac{c_\rho^2}{4} \right) + \left(2 + c_\rho + \frac{c_\rho}{6} \right)^2} \|x\| \\ &=: \left(\frac{V_g}{\rho_d} \right) \gamma \|x\|, \quad \forall x \in \Omega_c \end{aligned} \quad (\text{A10})$$

Therefore, $\dot{V} \leq -x^T x + 2\gamma \left(\frac{V_g}{\rho_d} \right) \|P\| \|x\|^2 = -\left(1 - 2\gamma \left(\frac{V_g}{\rho_d} \right) \|P\| \right) \|x\|^2 < 0$ is negative definite $\forall x \in \Omega_c$ if

$\|P\| < \frac{\rho_d}{2\gamma V_g}$ holds. Therefore, Ω_c is a compact positively invariant set and origin of Eq. (4) is an exponentially

stable equilibrium for any $x(0) \in \Omega_c$.

On the other hand, if $\sup_{t \geq 0} |V_t(t)| \leq V_{t_{\max}}$, then

$$\Delta f(x) = \begin{bmatrix} V_g \rho_e (1 - \cos \hat{\eta} \rho_d) / \rho_d \\ V_g \bar{\rho}^2 \sin \hat{\eta} \rho_d - \frac{V_g}{\rho_d} \hat{\eta} \end{bmatrix} + \begin{bmatrix} V_i \bar{\rho} \cos(\hat{\eta} \rho_d - \psi) / \rho_d \\ -V_i \bar{\rho}^2 \sin(\hat{\eta} \rho_d - \psi) \end{bmatrix} \quad (\text{A11})$$

Using Eq. (A10) we obtain that for $\forall x \in \Omega_c$

$$\begin{aligned} \|\Delta f(x)\| &\leq \left(\frac{V_g}{\rho_d} \right) \gamma \|x\| + \sqrt{(V_i \bar{\rho} \cos(\hat{\eta} \rho_d - \psi) / \rho_d)^2 + (V_i \bar{\rho}^2 \sin(\hat{\eta} \rho_d - \psi))^2} \\ &\leq \left(\frac{V_g}{\rho_d} \right) \gamma \|x\| + \sqrt{\left(\frac{V_i \bar{\rho}}{\rho_d} \right)^2 + (V_i \bar{\rho}^2)^2} = \left(\frac{V_g}{\rho_d} \right) \gamma \|x\| + \frac{|V_i| \bar{\rho}}{\rho_d} \sqrt{1 + \rho_d^2 \bar{\rho}^2} \\ &\leq \left(\frac{V_g}{\rho_d} \right) \gamma \|x\| + \frac{V_{t_{\max}} (1 + c_\rho)}{\rho_d^2} \sqrt{1 + (1 + c_\rho)^2} \end{aligned} \quad (\text{A12})$$

Now from Eq. (A1) an upper bound on $\dot{V}(x)$, $\forall x \in \Omega_c$ can be derived:

$$\begin{aligned} \dot{V}(x) &\leq -\left(1 - 2\gamma \left(\frac{V_g}{\rho_d} \right) \|P\| \right) \|x\|^2 + 2 \frac{V_{t_{\max}}}{\rho_d^2} (1 + c_\rho) \sqrt{1 + (1 + c_\rho)^2} \|P\| \|x\| \\ &= -\|x\| \left(\left(1 - 2\gamma \left(\frac{V_g}{\rho_d} \right) \|P\| \right) \|x\| - 2 \frac{V_{t_{\max}}}{\rho_d^2} (1 + c_\rho) \sqrt{1 + (1 + c_\rho)^2} \|P\| \right) \end{aligned} \quad (\text{A13})$$

Therefore, $\dot{V}(x) < 0$, $\forall x \in \Omega_c$ such that

$$\|x\| \geq \frac{2 \frac{V_{t_{\max}}}{\rho_d^2} (1+c_\rho) \sqrt{1+(1+c_\rho)^2} \|P\|}{1-2\gamma \left(\frac{V_g}{\rho_d} \right) \|P\|}$$

i.e.

$$\dot{V}(x) < 0, \frac{2 \frac{V_{t_{\max}}}{\rho_d^2} (1+c_\rho) \sqrt{1+(1+c_\rho)^2} \|P\|}{1-2\gamma \left(\frac{V_g}{\rho_d} \right) \|P\|} \leq \|x\| \leq \frac{c_\rho}{\rho_d} \quad (\text{A14})$$

Note Eq. (A14) is true if Conditions 1 and 2 hold since $\sqrt{\frac{\lambda_{\min}(P)}{\lambda_{\max}(P)}} \leq 1$. Let

$$\mu := \frac{2 \frac{V_{t_{\max}}}{\rho_d^2} (1+c_\rho) \sqrt{1+(1+c_\rho)^2} \|P\|}{1-2\gamma \left(\frac{V_g}{\rho_d} \right) \|P\|} \text{ and } \delta = \lambda_{\max}(P) \mu^2. \text{ Define } \Omega_\delta = \{x : \|x\| \leq \delta\}. \text{ Conditions 1 and 2}$$

guarantee that $\delta < c$ and therefore $\Omega_\delta \subset \Omega_c$. As a result we conclude that Eq. (10) is ultimately bounded in Ω_c ; more details can be found in Ref. 28.

Acknowledgments

This work was supported by the U.S. Government through funding from USSOCOM.

References

- ¹Whang, I.H., Dobrokhodov, V.N., Kaminer, I.I., Jones, K.D., "On Vision-Based Target Tracking and Range Estimation for Small UAVs," *Proceedings of AIAA Guidance, Navigation, and Control Conference*, San Francisco, CA, August 15-18, 2005.
- ²Dobrokhodov, V.N., Kaminer, I.I., Jones K.D., and Ghabcheloo, R., "Vision-Based Tracking and Motion Estimation for Moving Targets Using Small UAVs," *Proceedings of American Control Conference*, Minneapolis, June 2006.
- ³The PerceptiVU Target Tracking Software, PerceptiVU Inc, <http://www.PerceptiVU.com>.
- ⁴Hager, G., Hutchinson, S. and Corke, P., "A Tutorial Introduction to Visual Servo Control," *IEEE Transactions on Robotics and Automation*, 12(5) pp. 651-670, 1996.
- ⁵Mark, E. C., Matthew, W., "A Vision-Based Geolocation Tracking System for UAV's," *Proceedings of AIAA Guidance, Navigation, and Control Conference and Exhibit*, AIAA 2006-6246, Keystone, CO, 21 - 24 August 2006.

⁶Myungsoo, J., David, E. J. and Johnny, H. E., "Particle Filters for Target Tracking Using Vision Data for Micro-Air Vehicles," *Proceedings of AIAA Guidance, Navigation, and Control Conference and Exhibit*, AIAA 2006-6540, Keystone, Colorado, 21 - 24 August 2006.

⁷Call B., Beard, R.W, Taylorz, C., and Barber, B., "Obstacle Avoidance for Unmanned Air Vehicles Using Image Feature Tracking," *Proceedings of AIAA Guidance, Navigation, and Control Conference and Exhibit*, Keystone, CO, 21 - 24 August 2006.

⁸Koch, A., Wittich, H. and Thielecke, F., "A Vision-Based Navigation Algorithm for a VTOL - UAV," *Proceedings of AIAA Guidance, Navigation, and Control Conference and Exhibit*, AIAA 2006-6546, Keystone, CO, 21 - 24 August 2006.

⁹Watanabe, Y., Eric, N. J. and Calisez, A.J., "Vision-Based Guidance Design from Sensor Trajectory Optimization," *Proceedings of AIAA Guidance, Navigation, and Control Conference and Exhibit*, AIAA 2006-6607, Keystone, CO, 21 - 24 August 2006.

¹⁰Lili Ma, Stepanyan, V., Cao, C., Faruque, I., Woolsey, C. and Hovakimyan, N., "Flight Test Bed for Visual Tracking of Small UAVs," *Proceedings of AIAA Guidance, Navigation, and Control Conference and Exhibit*, AIAA 2006-6609, Keystone, Colorado, 21 - 24 August 2006.

¹¹Cao, C. and Hovakimyan, N., "Vision-Based Aerial Tracking Using Intelligent Excitation," *Proceedings of American Control Conference*, Portland, OR, USA, June 8-10 2005, pp. 5091–5096.

¹²Jones, G.C., Heyder-Bruckner, J.F., Richardson, T.S. and Jones, D.C., "Vision-based Control for Unmanned Rotorcraft," *Proceedings of AIAA Guidance, Navigation, and Control Conference and Exhibit*, -AIAA 2006-6684, Keystone, CO, 21 - 24 August 2006.

¹³Stepanyan, V., and Hovakimyan, N., "Visual Tracking of a Maneuvering Target," *Proceedings of AIAA Guidance, Navigation, and Control Conference and Exhibit*, AIAA 2006-671721, Keystone, CO, 24 August 2006.

¹⁴Stefan, F., "Robot Vision. Video-Based Indoor Exploration With Autonomous and Mobile Robots", Verlag: WILEY-VCH, ISBN: 3527405445.

¹⁵Redding, J., McLain, T.W., Beard, R.W., Taylor C., "Vision-Based Target Localization from a Fixed-Wing Miniature Air Vehicle," *2006 American Control Conference*, Minneapolis, MN, June 14-16, 2006.

¹⁶Brunke, S. and Campbell, M. E., "Square Root Sigma Point Filtering for Aerodynamic Model Estimation," *AIAA Journal of Guidance, Control, and Dynamics*, Vol. 27, No. 2, pp. 314–317, 2004.

¹⁷Campbell, M. E., Wheeler, M., "A Vision-Based Geolocation Tracking System for UAV's," *Proceedings of AIAA Guidance, Navigation, and Control Conference and Exhibit*, AIAA 2006-6246-691, Keystone, CO, 21 - 24 August 2006.

¹⁸Gibbins, D., Roberts, P., Swierkowski, L., "A Video Geo-location and Image Enhancement Tool for Small Unmanned Air Vehicles (UAVs)," *Proceedings of the Intelligent Sensors, Sensor Networks and Information Processing Conference*, 14-17 Dec. 2004.

¹⁹Doğançay, K., "On the Bias of Linear Least Squares Algorithms for Passive Target Localization," *Signal Processing archive*, Vol 84 , Issue 3, March 2004, pp 475 - 486.

²⁰Triggs, B., Laugier, V., "Automatic Camera Placement for Robot Vision Tasks", *Proceedings of 1995 IEEE International Conference on Robotics and Automation*, LIFIA-INRIA Rhone-Alpe, Grenoble, 21-27 May 1995, Vol: 2, pp. 1732-1737.

²¹Shima, T., Rasmussen, S.J, and Grossz, D., "Assigning Micro UAVs to Task Tours in an Urban Terrain," *Proceedings of AIAA Guidance, Navigation, and Control Conference and Exhibit*, AIAA 2006-6717, Keystone, CO, 21 - 24 August 2006.

²²Barron, J., Fleet, D., and Beauchemin, S., "Performance of Optical Flow Techniques," *International Journal of Computer Vision*, Vol. 12, No. 1, Feb 1994, pp. 43-77.

²³Shahraray, B. and Brown, M. K., "Robust Depth Estimation from Optical Flow," *IEEE Second International Conference on Computer Vision*, pp. 641-650, December 1988.

²⁴Rodriguez, A.F., Ready, B.R., Taylor, C.N., "Using Telemetry Data For Video Compression On Unmanned Air Vehicles," *Proceedings of AIAA Guidance, Navigation, and Control Conference and Exhibit*, AIAA 2006-6468, Keystone, CO, 21 - 24 August 2006.

²⁵Kaminer, I.I, Pascoal, A. M., Kang, W., Yakimenko, O.A, "Integrated Vision/Inertial Navigation Systems Design Using Nonlinear Filtering", *IEEE Transactions on Aerospace and Electronics*, Vol. 37, No.1, pp. 158-172, January 2001.

²⁶Hespanha, J.P, Yakimenko, O.A, Kaminer, I.I, Pascoal, A.M, "Linear Parametrically Varying Systems with Brief Instabilities: An Application to Integrated Vision / IMU Navigation", *IEEE Transactions on Aerospace and Electronic Systems Technology*, Vol 40, No 3, pp. 889-902, July 2004.

²⁷Olivera, P., Pascoal, A.M., Kaminer, I.I, "A nonlinear Vision-based Tracking System for Coordinated Control of Marine Vehicles," *Proceedings of the 10th Mediterranean Conference on Control and Automation – MED 2002*, Lisbon, Portugal, July 9-12, 2002.

²⁸Khalil, H.K, "Nonlinear Systems," Prentice Hall, 3rd edition, 2001.

²⁹Baer, W., "UAV Target Mensuration Experiment Using Synthetic Images from High Resolution Terrain Databases at Camp Roberts," 72nd MORSS, 10-12 June 2004, NPS Monterey, CA ,WG 25 T&E, <http://www.trac.nps.navy.mil/PVNT/>.

³⁰"Piccolo Family of Autopilots - Highly integrated autopilots for small UAVs," <http://cloudcaptech.com/>.

³¹Rothe, F., "Oscillations of the Taylor Polynomials for the Sin Function", NAW 5/1, No 4, December 2000, pp 397-398.